


Operational Modal Analysis of a Helicopter Rotor Blade Using Digital Image Correlation

S. Rizo-Patron¹ · J. Sirohi¹ 

Received: 12 May 2016 / Accepted: 10 October 2016 / Published online: 24 October 2016
© Society for Experimental Mechanics 2016

Abstract A novel procedure to perform operational modal analysis on a reduced-scale, 2 m diameter helicopter rotor blade is described. Images of the rotor blade rotating at 900 RPM are captured by a pair of high-speed digital cameras at a sampling rate of 1000 frames per second. From these images, the out-of-plane bending deformation of the rotor blade is measured using Digital Image Correlation, with a spatial resolution of 7.2 mm and an accuracy of 60 μm , or 0.006 % of the rotor radius. Modal parameters including natural frequencies and mode shapes are determined from the bending deformation through application of the Ibrahim Time Domain method. The first three out-of-plane bending modes were identified at each rotational speed and compared to an analytical finite element model of the rotor blade. The experimental and analytical natural frequencies agreed to within 0.2 % in the best case and 10.0 % in the worst case. The experimental mode shapes were also found to closely match the analytical predictions. The results of this study demonstrate the ability of this procedure to accurately determine the modal parameters of rotating helicopter rotor blades.

Keywords Digital image correlation · Helicopter blade deformation · Modal analysis · Rotating natural frequency · Rotating mode shape

Introduction

The dynamic response of typical rotating structures such as helicopter rotor blades and wind turbine blades is dominated by centrifugal force, which stiffens the rotor blades in flap (out of the rotor plane) bending, lead-lag bending (in the rotor plane) and torsion. This is especially important in cases where the structural flexural stiffness EI (E is the Young's modulus and I is the sectional moment of inertia) is comparable to the centrifugal stiffening $m_o\Omega^2R^4$ (m_o and R are the mass per unit length and radius of the rotor blade respectively, and Ω is the speed of rotation). As the rotational speed increases, the natural frequencies of the rotor blade increase. To validate analytical models, or for applications such as health monitoring, it is desirable to measure the natural frequencies and mode shapes of the rotor blade under rotation.

Modal analysis of rotating structures is a challenging area of research in structural analysis. The experimental determination of modal properties of a structure typically involves three steps (a) providing a known excitation, (b) measuring the resulting response and (c) extraction of modal properties from the measured response. Bucher and Ewins [1] present an overview of several techniques commonly used in experimental modal analysis of rotating structures. The primary difficulty in the case of a rotating structure is applying a known excitation to the system, which is required for frequency domain modal analyses. Another difficulty is installing sufficient sensors (such as strain gages) on the rotating blades to properly characterize the system. This installation is complicated by slip-rings to transmit electrical signals between the rotating and non-rotating frames. As a result, there are a limited number

✉ Jayant Sirohi
jayant.sirohi@mail.utexas.edu

¹ Department of Aerospace Engineering and Engineering Mechanics, The University of Texas at Austin, 210 E. 24th street, Austin, TX 78712, USA

of experimental modal analyses of rotating blades under operating conditions. Wilkie et al. [2] measured some natural frequencies of a 110 inch diameter model helicopter rotor blade at speeds ranging from 0 to 660 RPM, using strain gages bonded on the rotor blade at three spanwise locations. In this study, the mode shapes were not determined due to the limited spatial resolution of the measurements. Other sensing techniques have also been used to measure the blade deformation. Schroeder et al. [3] describe Fiber Bragg Gratings embedded in the blades of a 4.5 MW horizontal axis wind turbine to measure strain. Molenaar [4] describes the measurement of natural frequency on a non-rotating blade of a 750 kW horizontal axis wind turbine using accelerometers. These type of sensors also require some sort of interface, for electronics or for optics, between the non-rotating and rotating reference frames.

Recently, several researchers have used optical methods to measure the deformation of rotating wind turbine and helicopter rotor blades. Optical methods are attractive to measure deformation because they do not require electrical wiring and slip-rings, and they can be easily reconfigured to measure larger test articles. Abrego et al. [5] measured the displacement of the rotor blades of a full-scale UH-60A helicopter in a wind tunnel over a range of flight conditions using multi-camera photogrammetry. In this technique, high reflectance targets are attached to the test article. The position of the targets in the camera images is related to physical coordinates using a calibration. Ozbek et al. [6] used photogrammetry to measure the time history of blade deflection on a 2.5 MW horizontal axis wind turbine with a 80m diameter rotor. The advantage of optical techniques is that they are non-contact, they do not require expensive instrumentation to be installed on the blade, and they give very good accuracy, on the order of 1/5000 of the field of view for out-of-plane displacements. Digital Image Correlation is another optical technique that can measure displacements at a much higher spatial resolution. Baqersad et al. [7] reviewed several studies that used optical methods such as three-dimensional dynamic point tracking, stereophotogrammetry and Digital Image Correlation to measure the displacement of wind turbine blades, helicopter rotor blades and aircraft propeller blades. For example, Lundstrom et al. [8] performed an operational modal analysis on the rotor blade of a Robinson R44 helicopter in hover using stereophotogrammetry. In most of the studies on helicopter rotor blades, the measured deformation was used to extract natural frequencies and operating deflection shapes.

The present study describes operational modal analysis of the flap bending deformation of a blade from a 2.032

m diameter helicopter rotor at different rotational speeds. A jet of air is used to provide a forcing to the blade and the resulting flap bending free response is measured using Digital Image Correlation. The natural frequencies and mode shapes are extracted from these measurements using the Ibrahim Time Domain method. Previous studies on the modal analysis of rotating blades have involved photogrammetry and extraction of operating deflection shapes. In contrast, the present study combines a novel excitation technique, a high spatial resolution deformation measurement and time-domain modal analysis to extract natural frequencies and mode shapes of a rotating blade.

Methods

Digital Image Correlation

Digital image correlation (DIC) is an optical deformation measurement technique that can be used to measure the three-dimensional (3D), whole-field deformation of a body. Kahn-Jetter and Chu [9] describe the theory and application of 3D DIC. In this technique, a high-contrast speckle pattern is applied to the test article, and a pair of high-resolution cameras separated by a fixed distance captures images of the undeformed and deformed surface. A mapping function determined through a calibration procedure translates image coordinates into 3D physical coordinates. Cross-correlation of the undeformed and deformed images, in conjunction with the mapping function yields a deformation map of the surface.

This technique has been used for measuring the deformation of moving objects such as flapping wings [10–12] and rotating structures. For example, Ha et al. [12] used DIC to measure the natural frequencies, damping ratios and mode shapes of a flapping wing that was excited at its natural frequency using a shaker. Sirohi and Lawson [13] and Sicard and Sirohi [14] used DIC to measure the flap, lead-lag, and torsional deformation of rotating helicopter blades with diameters ranging from 7.6 cm to 61 cm rotating at 1500 RPM. It was found that out-of-plane deformations up to 10 mm could be measured with an accuracy of 97 μm , or 0.04 % of the rotor radius.

These studies on helicopter rotor blades validated the DIC measurement technique and established the achievable accuracy. However, in these studies, images were captured by low-speed digital cameras that were triggered at specific instants (azimuthal positions of the rotor blade), and the deformation was calculated by averaging the DIC results over 100 rotor revolutions. In the present study, time-resolved DIC is performed on a sequence of images of the rotor blade captured using high-speed digital cameras.



Modal analysis is then performed on the measured deformation to extract the natural frequencies and mode shapes of the rotating blade.

Ibrahim Time Domain Method

The Ibrahim Time Domain (ITD) [15] method of modal analysis was developed as an alternative to frequency domain modal analyses. One of the primary benefits of this method is that it does not require measurements of the excitation of the system under investigation. This makes it an ideal candidate for operational modal analysis of rotating blades, where the excitation is generally unknown and difficult to measure.

The ITD method requires measurement of the temporal response of the system at n locations and over $2m$ time instants (where $m > n$). These measurements can be assembled into a matrix Y of size $n \times 2m$ given by

$$Y = [y(t_1)y(t_2) \dots y(t_m)] \quad (1)$$

where the vectors y of size $n \times 1$ are the responses of the system at each time instant. Similarly, the matrices \bar{Y} and \hat{Y} can be assembled using measurements delayed in time by the sampling interval Δt as

$$\bar{Y} = [y(t_1 + \Delta t)y(t_2 + \Delta t) \dots y(t_m + \Delta t)] \quad (2)$$

$$\hat{Y} = [y(t_1 + 2\Delta t)y(t_2 + 2\Delta t) \dots y(t_m + 2\Delta t)] \quad (3)$$

These matrices can be combined into the response matrices $\hat{\Phi}$ and $\hat{\hat{\Phi}}$ (each of size $2n \times 2m$) where

$$\hat{\Phi} = \begin{bmatrix} Y \\ \bar{Y} \end{bmatrix} \quad \hat{\hat{\Phi}} = \begin{bmatrix} \bar{Y} \\ \hat{Y} \end{bmatrix} \quad (4)$$

An eigenvalue problem can be formulated from these response matrices:

$$A\Psi_r = \alpha_r\Psi_r \quad (5)$$

where the matrix A is calculated using a double least squares approximation as

$$A = \frac{1}{2} \left([\hat{\Phi}\hat{\Phi}^T][\hat{\Phi}\hat{\Phi}^T]^{-1} + [\hat{\hat{\Phi}}\hat{\hat{\Phi}}^T][\hat{\hat{\Phi}}\hat{\hat{\Phi}}^T]^{-1} \right) \quad (6)$$

Ibrahim [16] recommends keeping $m > 4n$ to ensure an accurate least squares approximation. The $2m$ eigenvectors $\{\Psi\}$ correspond to the mode shapes of the system, which appear as m complex conjugate pairs. The $2m$ eigenvalues α_r also appear as conjugate pairs and contain the corresponding natural frequencies and damping ratios. Thus, formulating these response matrices using the deformation measured at n locations will determine m modes.

Because of the overdetermined nature of the system, i.e., $m > n$, some of these modes are purely computational. This is advantageous in accounting for noise in the measured deformation. For example, if $p < n$ modes contribute to the measured response above the noise floor, then $m - p$ computational modes containing the measurement noise will be calculated. One method to separate the computational modes from the actual structural modes is to solve the eigenvalue problem for a different set of time instants and compare the complex eigenvectors from both solutions using the Mode Shape Correlation Constant (MSCC). Ibrahim and Pappa [17] define the MSCC as,

$$MSCC = \frac{|\{\gamma_1\}^T \{\gamma_2\}^*|^2}{\{\gamma_1\} \{\gamma_1\}^* \{\gamma_2\}^T \{\gamma_2\}^*} \quad (7)$$

where $\{\gamma_1\}$ is the first modal vector, $\{\gamma_2\}$ is the second modal vector, and $*$ denotes the complex conjugate. If two mode shapes have an MSCC close to 1.00, then the modes are correlated. This can be used to separate actual modes from computational modes, which will not be correlated between the two solutions.

Experiments

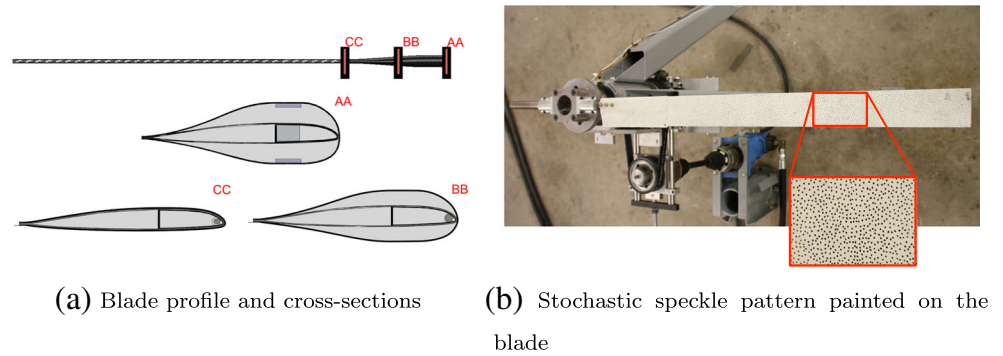
Experiments were performed to determine the modal parameters of a 2.032 m diameter composite helicopter rotor blade at rotational speeds up to 900 RPM. The goal of these experiments was to explore the ability of the ITD method in conjunction with DIC measurements to extract the natural frequencies and mode shapes of a rotating blade.

Experimental Setup

The test article was a single blade of a 2.032 m diameter rotor that was developed by Cameron et al. [18] for a reduced-scale counter-rotating coaxial helicopter rotor system. The rotor blade was mounted upside-down to a hub at a pitch angle of approximately 0 degrees to minimize rotor thrust and resultant bending of the rotor blade. A steel counterweight was mounted to the opposite side of the hub. The rotor blade has a chord length of 0.08 m and was spun by a hydraulic motor at rotational speeds up to 900 RPM, which corresponds to the test condition for the reduced-scale rotor system.

The composite rotor blade is composed of a foam core wrapped with several layers of carbon fiber composite, with an additional carbon fiber stiffening cuff near the root. A schematic of the rotor blade along with cross-sections at several spanwise locations is shown in Fig. 1a. A stochastic pattern of black speckles on a white matte background was applied to the blade for the DIC measurements (Fig. 1b).

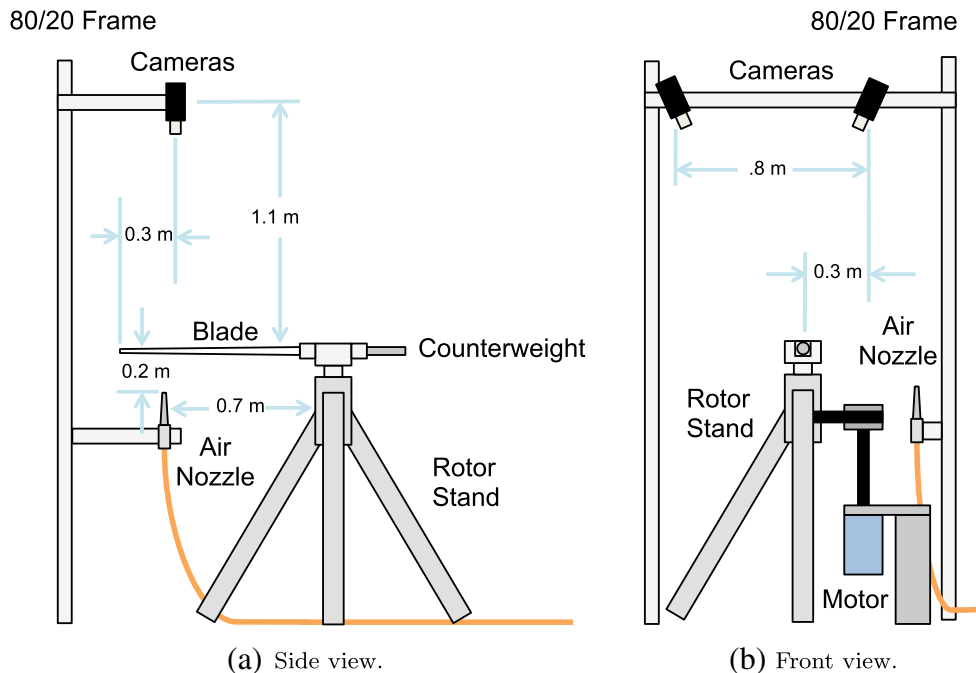


Fig. 1 Rotor blade test article

Images of the rotating blade were captured using a pair of Vision Research Phantom Miro M310 high-speed digital cameras. Each camera is capable of recording 3200 images per second at full (1280×800 pixel) resolution. The 25.6×16.0 mm CMOS camera sensor has a 12-bit resolution, and the minimum exposure time is $1 \mu\text{s}$. Images were processed using the LaVision DaVis 8.2.2 software package, which controlled the image capture and performed DIC on the saved images. The rotor blade was illuminated by a Dracast LED1000 Pro Daylight light panel, which provided flicker-free illumination, with additional lighting provided by a Smith Victor Q60 halogen light. Cameras and light fixtures were mounted to a 4.6 m tall frame assembled from 80/20 aluminum extrusions. A camera rail was mounted on extendable booms, which allowed the cameras to be placed directly over the rotor disk.

The rotor blade was excited by a nozzle from which a jet of compressed air passed through the rotor plane and perpendicular to it. As the blade passed through the jet of compressed air, it experienced a forcing that can be assumed to be impulsive in nature, thus exciting multiple structural modes. The hose pressure of the compressed air was approximately 6.2 bar (90 psi). The geometric arrangement of the cameras and rotor blade is shown in Fig. 2a and b. A picture of the test setup is shown in Fig. 3.

The image capture was synchronized with an external once-per-revolution trigger from a Hall Effect sensor on the rotor shaft. A single-axis piezoelectric accelerometer was used to monitor the vibration of the test stand during operation for safety. Signals from these two sensors were acquired with a National Instruments PXI-6358 data acquisition system and LabVIEW.

**Fig. 2** Schematic of test setup. The cameras are oriented such that the rotor blade enters the field of view when it is perpendicular to the plane of the cameras

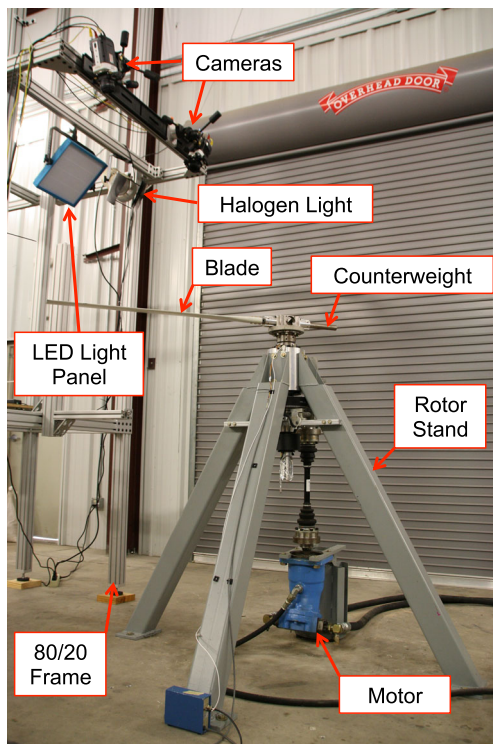


Fig. 3 Picture of test setup

Settings and Test Procedure

The speckles painted on the rotor blade were approximately 1 mm in diameter with 1–3 mm spacing between the speckles. With a 35 mm camera lens at a distance of 1.1 m, this corresponded to a speckle diameter of 2–3 pixels.

Before each test, a calibration of the system was performed to determine the mapping function to convert image coordinates to physical coordinates. Three images of a Type 1000 (0.8 m × 1 m) 2D calibration plate were averaged to produce the calibration image. The resultant standard error of fit was between 0.1 and 0.15 pixels.

First, a non-rotating test was performed by striking the blade at mid-span with an impulse hammer, and capturing 1200 images of the blade as it vibrated. Then, rotating tests were performed at several rotational speeds up to 900 RPM. At each rotational speed, 100 blade passages were recorded without any external excitation, and 500 blade passages were recorded with excitation provided by the air nozzle.

During each rotating test, images of the rotor blade were captured at fixed azimuthal positions for every revolution. The image capture was triggered once-per-revolution and a series of images were acquired starting when the rotor blade was approximately perpendicular to the plane containing the cameras. Thus, for a fixed rotational speed and image acquisition rate, images of the rotor blade were captured at the same azimuthal positions for every revolution.

The spacing of these azimuthal positions was determined by the rotational speed and the image acquisition rate.

The number of images that could be captured per revolution was determined by the field of view of the cameras. The cameras were able to view an area on the rotor plane of approximately 50 × 75 cm, which corresponded to an azimuthal range of 30 degrees. The outer 70 cm of the blade were contained in this field of view, including the outermost portion of the stiffening cuff.

At the maximum rotational speed of 900 RPM and at a 1000 frames per second (fps) image capture rate, 5 images were captured during each revolution before the rotor blade would move out of the field of view. A schematic of the image capture sequence is shown in Fig. 4. The aperture of the camera lens was set to 5.6 f/D and the exposure time was selected based on the maximum allowable blur at the tip of the blade, which was determined to be 1 mm (an exposure time of 11 μs at 900 RPM).

Postprocessing and Error Estimation

For the non-rotating test, the deformation was calculated relative to an image of the blade before it was impacted. At each rotational speed, the deformation was calculated at each azimuthal position, i.e., time instant, for both the unexcited and excited blade passages by averaging over all the revolutions. Only flap bending deformations were analyzed in this study.

The subset size (interrogation window size) for performing the DIC was set to 31 pixels. The step size was chosen to be 12 pixels, which corresponds to a 61 % overlap between windows. These settings produced a vector grid with a spatial resolution of 12 pixels, corresponding to a physical spatial resolution of 7.2 mm.

The ITD method was used to extract the natural frequencies and mode shapes from deformation vectors along spanwise strips (at constant chord locations of the rotor

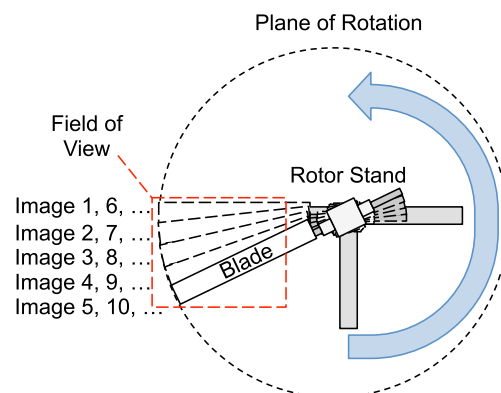


Fig. 4 Schematic of image capture sequence. The camera field of view is outlined in red

blade) of the produced vector field. To generate a set of modal parameters that could be statistically analyzed, the modal parameters were extracted from multiple strips of vectors at different chord locations. Additionally, the number of locations along each strip, the starting azimuthal position, and the ratio of time instants to measurement locations were varied. Computational modes were separated from structural modes by requiring modes from two different formulations to have an MSCC greater than 0.95 and frequencies matching to within 5%. The excitation of the rotor blade by the jet of air inherently creates a once-per-revolution forcing that appears in the response as a mode with a frequency equal to the rotational frequency and a damping ratio equal to zero. The once-per-revolution frequency and zero damping ratio are used to eliminate this forced mode from the results. Similarly, if any rotor harmonics appear in the response as integer multiples of the rotational frequency, they are also eliminated. Note that in most cases, the natural frequencies are not close to the operating frequency, so the rotor harmonics are not excited.

The nominal accuracy of the DIC measurements for these settings according to the LaVision user manual is $3\ \mu\text{m}$. However, previous experiments performed in our research group [14] determined an accuracy of $6\ \mu\text{m}$ for in-plane deformation and $60\ \mu\text{m}$ for out-of plane deformation. Therefore, in the present study, a bias error of $60\ \mu\text{m}$ is used for the flap bending deformation. The precision error is taken as the standard deviation over all measured rotor revolutions (100 revolutions in the unexcited cases and 500 revolutions in the excited cases). These two errors are combined (square root of the sum of the squares) to obtain the total experimental error, which is shown as error bars in the results below. The error in the extracted modal frequencies was determined based on a 95% confidence interval of the mean of the extracted frequencies over several numbers of rotor revolutions.

Results and Discussion

The average deformation of the rotor blade at 600 RPM, with and without excitation from the compressed air jet, is shown in Fig. 5 along with associated uncertainty. The baseline deformation of the rotor blade (unexcited condition) is due to a small amount of thrust produced by the cambered airfoil. The vibration resulting from the excitation is much smaller than the baseline bending deformation. For example, at the blade tip, the baseline deformation is approximately 8 mm, and the jet of air blowing upwards results in an upward vibratory deformation of approximately 2 mm. Some unusual deformation can be seen at a spanwise location around 550 mm; this is due to a region of glare on the rotor blades.

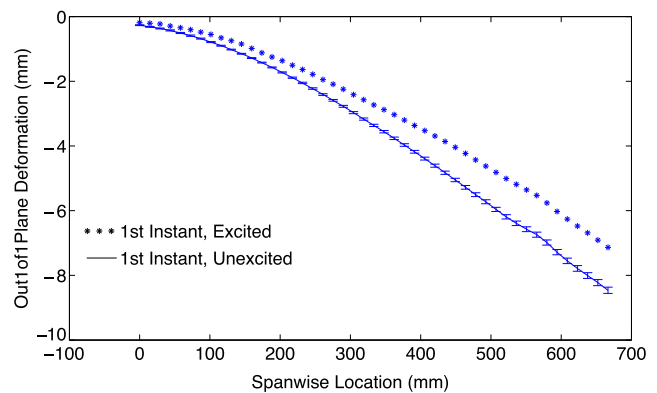


Fig. 5 Excited and unexcited blade deformations at 600 RPM

From the measured vibratory deformation, the natural frequencies and mode shapes of the first three flap bending modes of the blade were extracted using the ITD method. These were compared to an analytical model of the same rotor blade, developed by Schmaus and Chopra [19] using the University of Maryland Advanced Rotorcraft Code (UMARC). The analytical solution was developed by modeling the blade as a second-order, nonlinear, isotropic Euler-Bernoulli beam with flap, lead-lag, torsion, and axial motion, and solving the equations of motion using the finite element method. The analysis was adjusted so that the non-rotating flap bending frequencies matched the non-rotating frequencies measured from the rap test; in this way, realistic boundary conditions were captured in the analysis.

A fan plot comparing the analytical (UMARC predictions) and experimental (extracted from measurements using ITD method) natural frequencies as a function of rotational speed is shown in Fig. 6. The frequencies in the fan plot are normalized by 900 RPM, which is the design speed of the rotor. That is, the x -axis indicates the rotational speed

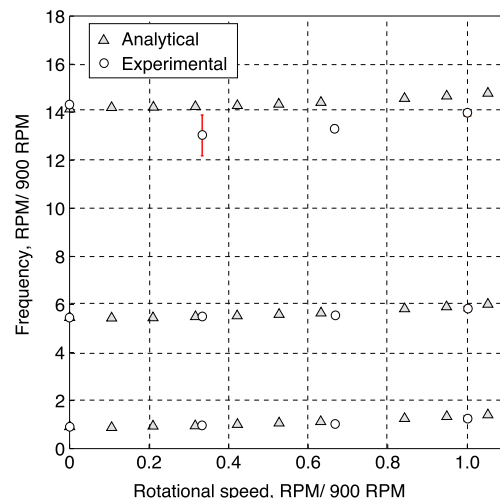


Fig. 6 Comparison of analytical and experimental flap bending natural frequencies as a function of rotational speed

Table 1 Comparison of analytical and experimental natural frequencies

Mode		0 RPM	300 RPM	600 RPM	900 RPM
First flap	Analytical (Hz)	13.6	14.4	15.6	20.9
	Experimental (Hz)	13.6±0.01	14.5±1.2	14.9±0.8	18.8±1.6
	% difference	0.0 %	0.6 %	4.3 %	10.0 %
Second flap	Analytical (Hz)	81.6	82.4	84.2	89.4
	Experimental	81.9±0.01	82.6±0.8	83.1±0.6	88.0±1.9
	% difference	0.3 %	0.2 %	1.3 %	1.6 %
Third flap	Analytical (Hz)	212.8	213.6	216.1	221.0
	Experimental	214.8±0.3	195.5±12.7	199.8±2.0	209.7±1.9
	% difference	0.9 %	8.5 %	7.5 %	5.1 %

of the rotor as a fraction of the nominal design speed. They y-axis indicates the natural frequency of a particular mode as a fraction of the nominal rotor speed. It can be seen that the lowest frequency mode, which corresponds to the fundamental flap bending mode, occurs at approximately once per revolution. The natural frequencies of all three modes increase with increasing rotational speed due to the stiffening effect of centrifugal acceleration.

The natural frequencies are summarized in Table 1. In general, the experimental natural frequencies show excellent agreement with the analytical predictions, especially at low rotational speeds, and also exhibit the expected trend

of increasing natural frequency with increasing rotational speed. The only discrepancy with this expected trend is for the third natural frequency at 300 RPM; however, this point also has the most error (largest error bar).

The first flap bending frequency at 900 RPM was the furthest from the predicted value with a 10 % difference between the experiments and analysis. This is a result of the sampling frequency used to capture the images. At a sampling frequency of 1000 fps, insufficient displacement occurs between each time shifted response matrix. This leads to errors in the determination of modal parameters.

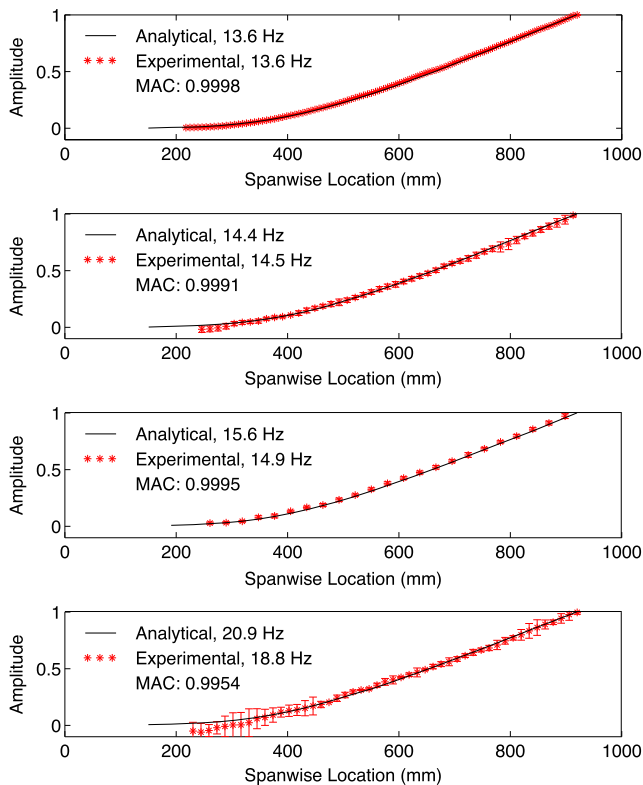


Fig. 7 First flap bending mode shapes. First plot is at 0 RPM, second is at 300 RPM, third is at 600 RPM, fourth is at 900 RPM

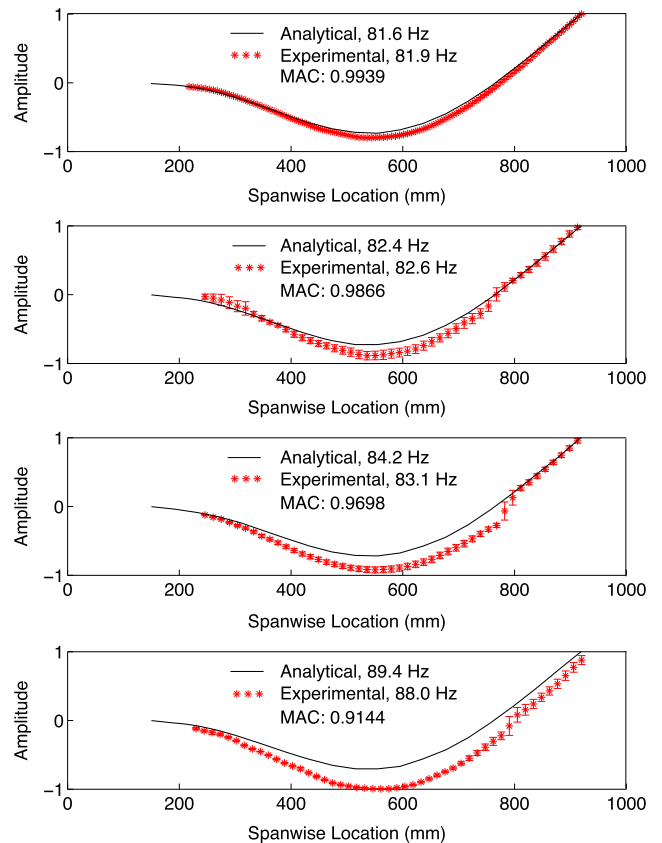


Fig. 8 Second flap bending mode shapes. First plot is at 0 RPM, second is at 300 RPM, third is at 600 RPM, fourth is at 900 RPM



In general, the sampling frequency should be less than 100 times the frequency of interest. However, if the sampling frequency is too low, the blade will move out of the camera field of view before enough images can be captured to formulate the response matrices. Therefore, the images that were captured at 1000 fps were down-sampled as needed for different test cases.

The jet of air was located near the tip of the rotor blade and was therefore not as effective in exciting the third mode as the first two modes. As a result, the third mode was more difficult to resolve accurately using the ITD analysis and these results exhibit the most scatter.

The first flap bending mode shape at each rotational speed extracted from the experimental measurements (using the ITD method) is shown in Fig. 7, along with the analytical prediction (from UMARC). There is excellent agreement between the experiment and the analysis at all rotational speeds. The experimental error increases with increasing rotational speed and is larger closer to the root of the blade, where deflections are smaller. The extracted mode shapes do not have the same number of spanwise points, because the ITD method was run with different spatial resolutions (obtained by resampling the data) and the mode shape with the highest MSCC was retained. The analytical and experimental mode shapes were quantitatively compared using the

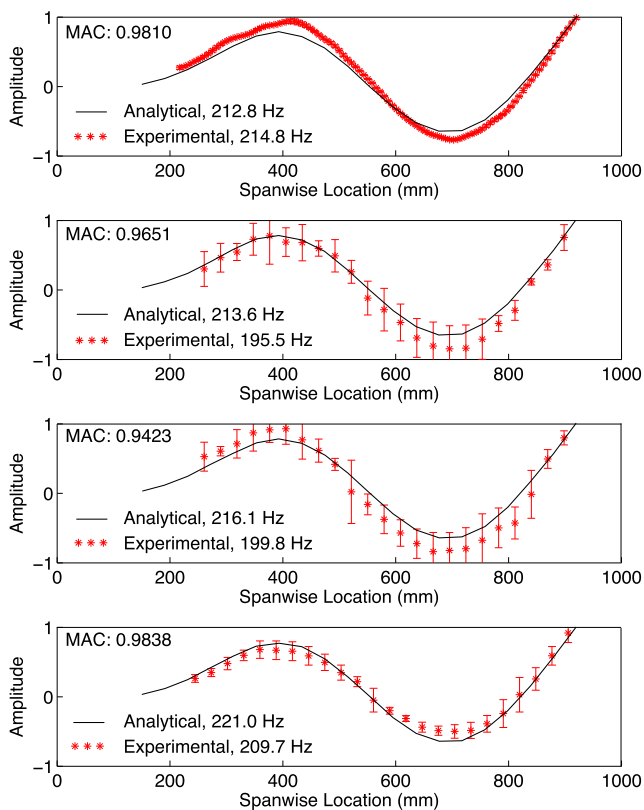


Fig. 9 Third flap bending mode shapes. First plot is at 0 RPM, second is at 300 RPM, third is at 600 RPM, fourth is at 900 RPM

Modal Assurance Criterion (MAC) [20], (which is the same as the MSCC), and these values are also shown in each plot. It can be seen that the lowest MAC of 0.9954 occurs at the highest rotational speed; note that any value of MAC greater than 0.9 is considered as a very good agreement between the compared mode shapes.

The second flap bending mode shapes are shown in Fig. 8. For every rotational speed, the second flap bending mode was the best resolved and most repeatable mode shape. However, as the rotational speed increases, the difference between the experiment and the analysis increases. The slight discontinuity in the mode shape at the node near the tip is an artifact of the spatial resolution and the method of approximating real-valued mode shapes from complex mode shapes. The minimum MAC in the case of the second mode is 0.9144 and occurs at the highest rotational speed.

The third flap bending mode shapes are shown in Fig. 9. There is good agreement between experiment and analysis even though the spanwise location of the jet of air did not provide much excitation to the third bending mode. The lowest MAC of 0.9423 occurs at the rotational speed of 600 RPM.

Summary and Conclusions

The flap bending deformation of a rotating helicopter blade was measured using DIC over a range of 0 RPM to 900 RPM. The first three flap bending natural frequencies and mode shapes were extracted from these measurements using the ITD method, and were compared to an analytical model of the system (finite element method). The analytical and experimental natural frequencies showed excellent agreement, especially for the non-rotating test and the second flap bending mode for the rotating test. The non-rotating frequencies matched to within 0.9 %, and the rotating second mode natural frequencies matched to within 1.6 %. The first flap bending mode at 900 RPM had the largest deviation (10%) between the analytical and experimental frequencies. The uncertainty of the natural frequencies ranged from 0.1 % for the third mode at 0 RPM to 8.5 % for the first mode at 900 RPM. The average uncertainty of the mode shapes ranged from 0.09 % for the first mode at 0 RPM to 5.6 % for the third mode at 600 RPM.

This study describes the first integration of DIC with ITD method for modal analysis of a rotating helicopter blade. The results suggest that this operational modal analysis procedure is an effective method to experimentally determine the modal parameters of helicopter rotor blades in the operating condition. While the results from this study are promising, there are several aspects of the experimental procedure that may be improved to increase the accuracy, repeatability, and functionality of the results.

The current method of excitation provides a single impulse per revolution. This produces a strong forcing mode that can be difficult to separate from the first flap bending mode. This issue can be alleviated by applying the forcing at an arbitrary time and acquiring data until the transient has died down, before applying the next forcing. To perform DIC on the blade at higher rotational speeds, the camera exposure time must be decreased to reduce tip blur. This would require more intense lighting, or the test article could be speckled with a fluorescent dye such as Rhodamine and illuminated using a laser source. Increasing the field of view will enable capture of more angular indices for the formulation of response matrices. Capturing more images per revolution allows the user to artificially decrease the sampling rate by selecting every second, third, fourth, etc. time instant to analyze in the ITD method. This would allow the lower natural frequencies to be accurately identified at higher rotational speeds. The field of view can be increased by increasing the camera to test article distance; however, this must be balanced against the resulting loss of spatial resolution and accuracy.

Acknowledgments This material is based upon work supported by, or in part by, the U. S. Army Research Laboratory and the U. S. Army Research Office under contract/grant number W911NF-13-1-0463, with Dr. Matthew Munson as Program Manager.

References

1. Bucher I, Ewins DJ (2001) Modal analysis and testing of rotating structures. *Philos Trans R Soc London, Ser A Math Phys Eng Sci* 359(1778):61–96
2. Wilkie WK, Mirick PH, Langston CW (1997) Rotating shake test and modal analysis of a model helicopter rotor blade. Technical Report NASA TM 4760, National Aeronautics and Space Administration, Langley Research Center, Hampton, Virginia 23681
3. Schroeder K, Ecke W, Apitz J, Lembke E, Lenschow G (2006) A fibre bragg grating sensor system monitors operational load in a wind turbine rotor blade. *Meas Sci Technol* 17(5):1167
4. Molenaar DP (2003) Experimental modal analysis of a 750 kw wind turbine for structural model validation. In: *ASME Wind Energy Symposium*, pages 332–339. American Society of Mechanical Engineers, p 2003
5. Abrego AI, Olson LE, Romander EA, Barrows DA, Burner AW (2012) Blade displacement measurement technique applied to a full-scale rotor test. In: *American Helicopter Society 68th Annual Forum*, Fort Worth, Texas, May 1–3
6. Ozbek M, Rixen DJ, Erne O, Sanow G (2010) Feasibility of monitoring large wind turbines using photogrammetry. *Energy* 35(12):4802–4811
7. Baqersad J, Poozesh P, Niezrecki C, Avitabile P (2016) Photogrammetry and optical methods in structural dynamics - a review. *Mech Syst Signal Process*:–
8. Lundstrom T, Baqersad J, Niezrecki C (2013) Special Topics in Structural Dynamics. In: *Proceedings of the 31st IMAC, A Conference on Structural Dynamics, 2013*, chapter Using High-Speed Stereophotogrammetry to Collect Operating Data on a Robinson R44 Helicopter, pages 401–410. Springer New York, New York, NY, vol 6
9. Kahn-Jetter ZL, Chu TC (1990) Three-dimensional displacement measurements using digital image correlation and photogrammetric analysis. *Exp Mech* 30(1):10–16
10. Wu P, Ifju P, Stanford B (2010) Flapping Wing Structural Deformation and Thrust Correlation Study with Flexible Membrane Wings. *AIAA J* 48(9):2111–2122
11. Tran J, Sirohi J, Gao H, Wei M (2015) Reduced-order modeling of loads and deformation of a flexible flapping wing. In: *AIAA 2015-0177, 56th AIAA/ASCE/AHS/ASC Structures, Structural Dynamics, and Materials Conference*, Kissimmee, Florida, Jan. 5–9
12. Ha NS, Vang HM, Goo NS (2015) Modal analysis using digital image correlation technique: An application to artificial wing mimicking beetle's hind wing. *Exp Mech* 55(5):989–998
13. Sirohi J, Lawson MS (2012) Measurement of helicopter rotor blade deformation using digital image correlation. *Opt Eng* 51(4):043603–1
14. Sicard J, Sirohi J (2013) Measurement of the deformation of an extremely flexible rotor blade using digital image correlation. *Meas Sci Technol* 24(6):065203
15. Ibrahim SR, Mikulcik EC (1977) A method for the direct identification of vibration parameters from the free response. *Shock and Vibration Bulletin. Bulletin*:47
16. Ibrahim SR (1986) Double least squares approach for use in structural modal identification. *AIAA J* 24(3):499–503
17. Ibrahim SR, Pappa RS (1982) Large modal survey testing using the ibrahim time domain identification technique. *J Spacecr Rocket* 19(5):459–465
18. Cameron CG, Karpatne A, Sirohi J (2016) Performance of a mach-scale coaxial counter-rotating rotor in hover. *J Aircr*:1–10
19. Schmaus J, Chopra I (2015) Performance and loads prediction for a high advance ratio coaxial rotor
20. Allemang RJ (2003) The Modal Assurance Criterion – Twenty Years of Use and Abuse. *Sound Vib* 37(8):14–23